Association Kinetics for Perfluorinated *n*-Alkyl Radicals

Hrishikesh Ram,[*,†,‡,¶] Yuri Georgievskii,[¶] Sarah N. Elliott,[¶,§] and Stephen J. Klippenstein[¶]

†Department of Chemistry, North Carolina State University, Raleigh, North Carolina 27606, United States

‡Department of Chemical and Biomolecular Engineering, North Carolina State University, Raleigh, North Carolina 27606, United States

¶Chemical Sciences and Engineering Division, Argonne National Laboratory, Lemont, Illinois 60439, United States

§Dipartimento di Chimica, Materiali e Ingegneria Chimica "Giulio Natta", Politecnico di Milano, Milano, Italia

E-mail: hram@ncsu.edu

Abstract

Radical-radical reaction channels are important in the pyrolysis and oxidation chemistry of perfluoroalkyl substances. In particular, unimolecular dissociation reactions within unbranched n-perfluoroalkyl chains, and their corresponding reverse barrierless association reactions, are expected to be significant contributors to the gas-phase thermal decomposition of families of species such as perfluorinated carboxylic acids and perfluorinated sulfonic acids. Unfortunately, experimental data for these reactions are scarce and uncertain. Furthermore, obtaining reliable theoretical predictions for such reactions is a laborious and computationally intensive task. In this work, we present state-of-the-art *ab initio* transition-state-theory-based master-equation calculations examining the chemical kinetics of the various association/decomposition reactions producing/decomposing the $C_2 - C_4$ series of unbranched n-perfluoroalkanes (C_2F_6, C_3F_8, and C_4F_{10}). The variable-reaction-coordinate transition-state theory (VRC-TST) formalism is employed in computing the microcanonical and canonical rates for the association reactions. Reaction thermochemistry is obtained via composite quantum chemistry calculations and the laddering of error-cancelling reaction schemes via a connectivity-based hierarchy approach employing ANL1/ANL0-style reference energies. Lennard-Jones collision model parameters for the considered systems were estimated by a direct dynamics approach, and collisional energy transfer parameters were obtained from analogies to systems of similar size and heavy-atom connectivity. A one-dimensional master equation approach was used to convert the microcanonical rate coefficients from the VRC-TST analysis into temperature- and pressure-dependent rate constants for the association reactions and the reverse dissociation reactions. The data are reported in standardized formats for usage in comprehensive chemical kinetic models for PFAS thermal destruction.

Keywords: PFAS, Radical Association, Kinetics, VRC-TST, Master Equation, Thermochemistry

1. Introduction

The thermal destruction of perfluoroalkyl substances (PFAS) has garnered much attention recently due to concerns of adverse health effects, environmental bioaccumulation, and long half-lives.[1–5] Full mineralization of all $C-F$ bonds into HF and CO_2 is necessary for effective removal of PFAS from contaminated matrices, but the combustion is often incomplete. The difficulty in experimentally characterizing the products of incomplete combustion, which are potentially hazardous, has prompted a variety of computational studies into the chemical reaction mechanisms of PFAS pyrolysis and oxidation.[6–10]

Extensive examinations of the thermochemistry of species involved in the destruction of perfluorinated carboxylic acids and perfluorinated sulfonic acids indicate that radical-radical reaction channels, such as homolytic dissociation within perfluoroalkyl chains, are likely important alongside molecular or pericyclic reactions with sufficiently low electronic barriers to contribute at incineration conditions. However, in the existing theoretical studies on PFAS thermal decomposition, the consideration of barrierless reactions has been limited. An example is the variational transition-state theory treatment of reactions like fluorine atom loss or singlet-CF_2 dissociation from n-perfluoroalkyl radicals or the dissociation of the carbon-sulfur bond in perfluorinated sulfonic acids, using bond-stretching coordinates and single-reference density functional methods by Altarawneh and co-workers.[7,8] While these reactions may be relevant to PFAS thermal decomposition, the series of carbon-carbon bond scissions (and their reverse associations) within perfluoroalkyl chains indicated to be important by bond dissociation energies have not been studied thoroughly. Wardlaw and co-workers have carried out a theoretical study of $2\,CF_3 \rightleftharpoons C_2F_6$ using canonical flexible transition state theory,[11] but more refined theoretical studies of this reaction and studies of the size dependence of perfluoroalkyl radical combinations have not been published to our knowledge.

Obtaining reliable kinetic parameters for radical-radical reaction channels from theoretical calculations is difficult, as they are barrierless, and the radical-radical interaction potential in

the transition state region exhibits strong multireference electronic character. Furthermore, a number of the modes are strongly coupled with significant deviation from harmonic oscillator behavior. The prediction of the pressure dependence is complicated by the dependence on thermochemical data and energy transfer parameters.[12] Experimental kinetics data are sparsely available for radical-radical pathways due to the challenges of generating and monitoring radicals and the complications of secondary reactions. As a result, the experimental data that are available often display high uncertainty.

In the interest of developing a complete high fidelity combustion kinetics model for PFAS, we have undertaken a study of reactions R1 – R5 below. Reactions R1 – R4 are the association reactions of the $C_1 - C_3$ unbranched n-perfluoroalkyl radicals to form the $C_2 - C_4$ unbranched n-perfluoroalkanes. Reaction R5 is the bimolecular well-skipping reaction over the C_4F_{10} well.

$$2\,CF_3 \underset{k_{-1}}{\overset{k_1}{\rightleftharpoons}} C_2F_6 \tag{R1}$$

$$CF_3 + C_2F_5 \underset{k_{-2}}{\overset{k_2}{\rightleftharpoons}} C_3F_8 \tag{R2}$$

$$CF_3 + C_3F_7 \underset{k_{-3}}{\overset{k_3}{\rightleftharpoons}} C_4F_{10} \tag{R3}$$

$$2\,C_2F_5 \underset{k_{-4}}{\overset{k_4}{\rightleftharpoons}} C_4F_{10} \tag{R4}$$

$$CF_3 + C_3F_7 \underset{k_{-5}}{\overset{k_5}{\rightleftharpoons}} 2\,C_2F_5 \tag{R5}$$

High-pressure-limit rate coefficients for the association reactions were obtained using a rigorous direct dynamics approach within the variable-reaction-coordinate transition-state theory (VRC-TST) formalism. Thermochemistry was calculated using composite schemes, laddered to reduce uncertainties, and collisional energy transfer parameters were evaluated both by direct dynamics and by analogy to similar systems. Then, a master equation (ME) approach was used to obtain the reverse dissociation rate constants and examine the falloff behavior.

4

2. Methods

2.1 High-Pressure-Limit Rate Coefficients

2.1.1 VRC-TST

The barrierless nature of radical-radical reactions correlates with a large variation in the location and form of the transition state dividing surface with excess energy. In particular, at low temperatures, enthalpic effects are most important and the transition state lies at large radical-radical separations. At higher temperatures, the decrease in entropy with decreasing separation pushes the transition state towards shorter separations. Within variational transition-state theory (VTST), the variationally optimal estimate for the reactive flux is provided by its minimum with respect to some reaction coordinate such as the separation distance.

The traditional procedure for implementing VTST assumes that rigid-rotor harmonic-oscillator (RRHO) approximations (with corrections, such as hindered-rotor assumptions for intermolecular bending modes) are valid along a minimum-energy reaction path (RP), and relies on determination of normal-mode harmonic frequencies and moments of inertia along the reaction path. This approach is thus known as RP-VTST.[13]

For radical-radical reactions, the transition state typically lies at separations where the radical-radical bending motions are not well described as either harmonic oscillators or free rotors. An alternative procedure called "flexible TST" uses an approximate separation into what are essentially "conserved" vibrational modes of the radicals and the remaining "transitional" modes describing the relative and overall rotations of the radicals.[14,15] This separation allows for a fully-coupled anharmonic treatment of the radical-radical bending and rotational degrees of freedom. Within this approach, the number of energetically accessible quantum states of the transition state for a given energy E and total angular momentum J, $N^{\ddagger}(E, J)$, can be evaluated as a convolution of a direct quantum sum for the conserved mode contribution with a classical phase-space-integral (PSI) treatment of the transitional

5

mode contribution. This approach is popular for its accurate treatment of issues involving low-frequency modes. However, in its original formulation, it assumes that the reaction coordinate is defined by the radical-to-radical center-of-mass separation distance, which fails at short separations, especially when the reactive site is far from the center-of-mass within a given fragment.[16]

The variable-reaction-coordinate (VRC) approach[17–21] represents an improvement on the center-of-mass-based flexible TST by incorporating variation in the reaction coordinate definition as well. In other words, both the value and the definition of the reaction coordinate are variationally optimized, affording superior descriptions of the reaction coordinate at short fragment separation, while retaining the classical PSI treatment of transitional mode contributions. Monte Carlo sampling of the transitional modes and subsequent integration of the classical PSI representation of the transition-state partition function, are commonly carried out via direct dynamics (i.e., with "on-the-fly" potential evaluations of the sampled geometric orientations).[16] The optimal dividing surface at a given temperature T is obtained by variationally minimizing the resulting fragment association rate coefficient with respect to both the value and the definition of the generalized reaction coordinate.

Within the VRC-TST approach, the radicals are assumed to rotate about arbitrarily located "pivot points". The reaction coordinate is then defined in terms of a fixed separation between these pivot points. The full variational optimization then is carried out for both the pivot point location and the separation between them. These optimizations are usually accomplished through grid-based evaluations of the numbers of available states, $N^{(E,J)}$. In some instances, it is effective to include multiple pivot points on each radical, which leads to a multifaceted transition-state dividing surface.[19]

In this work, we employed the VRC-TST approach with direct evaluations of the interaction energies (using multireference electronic structure theory as described in the following subsection). The pivot points were placed either directly at the location of the radical site on each fragment, or on both faces of the reacting fragment at distances ranging from 0.26

6

to 0.79 Å from the radical site and along the appropriately defined axis. As many as 48 dividing surfaces were constructed for each reaction by considering point-to-point separation distances ranging from 2.1 to 10.6 Å. Monte Carlo orientational sampling was terminated upon achieving integration uncertainties below a 3% threshold, sometimes requiring as many as $4000-5000$ samplings and single-point energy evaluations for each face of a given dividing surface.

2.1.2 Radical-Radical Interaction Potentials

The nature of the radical-radical interaction potential in the transition-state region (roughly $2-5$ Å, where the magnitudes of long-range van der Waals and bonding forces are similar) requires the use of multireference methods in the direct potential evaluations. Here, these direct potential evaluations in the VRC-TST calculations were carried out using complete-active-space second-order perturbation theory (CASPT2).[22] Fragments were kept rigid in their asymptotic equilibrium geometries, obtained at the same level of theory. Active spaces for all multireference calculations described in this work were chosen to be (2e,2o), in order to allow the molecule to properly dissociate into fragment radicals at large separations. Based on prior literature on multireference potential energy surfaces using VRC-TST,[23] a real level shift of 0.2 and an ionization potential electron affinity (IPEA) shift of 0.25 eV were used for all complete-active-space calculations.

For computational feasibility, the cc-pVDZ basis set was used in the direct potential evaluations. Higher accuracy is obtained by accounting for limitations in (i) the CASPT2 method, (ii) the small cc-pVDZ basis set, and (iii) fragment geometry relaxation effects, through the development of orientation-independent one-dimensional correction terms. These correction term evaluations are based on explicit calculations for R1, as a function of the radical-radical separation distance, R_{CC}. To correct for method and basis set limitations, a fully-relaxed minimum energy path (MEP) for $2\,CF_3 \rightleftharpoons C_2F_6$ was constructed in D_{3d}-symmetry using the explicitly-correlated CASPT2-F12 method[24] with the aug-cc-pVTZ-F12

7

basis set.[25–27] Single-point energies along this fully-relaxed MEP were obtained using explicitly-correlated and Davidson-corrected multireference configuration interaction with the same basis set, MRCI-F12+Q/aug-cc-pVTZ-F12.[28–32]

Additionally, a so-called "spin-splitting" approach was also used, taking advantage of the use of high-accuracy single-reference methods to describe the energy of the triplet state along the MEP.[12,33] The energy of the triplet state was evaluated using explicitly-correlated coupled-cluster theory with single and double excitations and perturbative connected triples, employing a restricted spin Hartree-Fock reference wavefunction, RHF-UCCSD(T)-F12b,[34–36] along with an aug-cc-pVTZ-F12 basis. Then, the energy of the singlet state was obtained by calculating singlet-triplet energy gaps using both of the high-accuracy multireference methods considered, CASPT2-F12/aug-cc-pVTZ-F12 and MRCI-F12+Q/aug-cc-pVTZ-F12. These spin-splitting-based values are expected to be less sensitive to the multireference method used for singlet-triplet gaps. An average of the two spin-splitting approaches is used as the final reference energy in determining the correction potential.

The accuracy and uncertainty of the various correction potentials in the transition state region is discussed in **Section 3.1**. The final correction potential is taken as the difference between the average spin-splitting energies on the relaxed CASPT2-F12/aug-cc-pVTZ-F12 MEP geometries and the CASPT2/cc-pVDZ energies along a constrained D_{3d} MEP in which the asymptotic equilibrium CASPT2/cc-pVDZ radical geometries were kept rigid.

The magnitude and importance of geometry relaxation effects for perfluoroalkyl radical combinations can be separately gauged entirely at the CASPT2/cc-pVDZ level, through the evaluation of the constrained rigid MEPs previously mentioned. In other words, the geometry relaxation component to the total correction is simply the difference between relaxed and rigid MEPs at CASPT2/cc-pVDZ as a function of the separation distance. The implications of this analysis are further discussed in **Section 3.1**.

Due to the large size of the considered systems, we were forced to use a more internally-contracted version[37] of CASPT2 for the potential evaluations for R2 – R4. Since geometry

8

relaxation effects were not expected to change significantly and the explicitly-correlated methods with large basis sets were computationally infeasible for these systems, we chose to apply the correction potential obtained for $2\,CF_3 \rightleftarrows C_2F_6$ to all the reactions considered.

This approach has been successful before when applied to similar alkyl-alkyl analogues.[21] The rate coefficients include an electronic degeneracy correction of 1/4 to account for the reaction occurring solely on the ground singlet spin state. For the self-association reactions R1 and R4, an additional correction factor of 1/2 was applied to account for symmetry effects. Finally, a dynamical correction factor of 0.85 was applied across all cases to account for recrossing effects.[21,38]

2.2 Thermochemistry

The high-pressure limit for the reverse dissociation rate constants have a strong sensitivity to reaction enthalpies, as do the pressure-dependent rate constants in both directions. Thus, it is desirable to obtain high accuracy estimates for the reaction enthalpies. To this end, we used the connectivity-based hierarchy (CBH) technique[39] for systematically constructing error-cancelling reaction schemes in conjunction with the laddered CBH-ANL approach.[40] The first (CBH0), second (CBH1), third (CBH2), and fourth (CBH3) rungs of the CBH schemes have been used in this work. These reactions would fall under the "isogyric", "isodesmic", "hypohomodesmotic"/"isoatomic", and "hyperhomodesmotic" reaction classes respectively, in the hierarchy put forth by Wheeler et al.[41] As shown in the **Supporting Information**, CBH0 was used for the target species CF_3, CBH2 for C_2F_5 and C_2F_6, and CBH3 for C_3F_7, C_3F_8 and C_4F_{10}. The required reference species for these schemes have also been considered as shown in **Table S1**. A laddering scheme of successive quantum chemistry methods was used to construct the different CBH level references. CBH0 reference species for each element in consideration (H, C, and F) were selected as H_2, CH_4, and HF, for which enthalpies of formation at 0 K were sourced from the Active Thermochemical Tables (ATcT), V1.202.[42–44] We also used ATcT values for H to define a reference radical enthalpy of formation.

9

2.2.1 Composite Electronic Structure Theory

The thermochemistry was calculated according to a set of high-level composite quantum chemistry methodologies based on a CCSD(T)/CBS+HOE+CV+REL+DBOC+SO+ZPVE+ANH strategy (outlined below) inspired by the ANL0/ANL1 family of methods.[45] The method at which every component of each CBH reaction energy was obtained is outlined in **Table S1**, using abbreviations for the basis sets. For each entry in **Table S1**, the single-point energies for all the species used in the given CBH scheme were treated at the specified level of theory, using converged minimum structures at the level of theory indicated for geometries.

For the smaller systems, the basis CBH reaction energies have been obtained from CCSD(T) energies at the complete-basis-set, CBS, limit computed using either RHF-UCCSD(T)-F12b/cc-pVnZ-F12 or RHF-UCCSD(T)/aug-cc-pVnZ. The cc-pVnZ-F12 series provided more rapid basis set convergence, but for some of the smaller species it appears that the aug-cc-pVnZ series provided more reliable convergence. For robustness where possible, both estimates of the CCSD(T)/CBS energies were computed and averaged. Up to the cc-pV5Z-F12 and aug-cc-pV6Z basis sets have been used. For larger systems, RHF-UCCSD(T)-F12b/cc-pVnZ-F12 energies (with CBS extrapolation where possible) were used.

A correction term for higher-order excitations, HOE, was incorporated whenever computationally feasible by taking the difference of UHF-UCCSDT(Q) and RHF-UCCSD(T) energies at the cc-pVnZ basis, and if possible, the difference of UHF-UCCSDTQ(P) and UHF-UCCSDT(Q) energies as well.[46,47] Core-electron correlation and core-valence interactions, CV, are accounted for by a correction term composed of the difference between all-electron RHF-UCCSD(T,Full) calculations and frozen-core RHF-UCCSD(T) calculations using the cc-pwCVnZ or aug-cc-pwCVnZ basis sets.[48] The aug-cc-pwCVnZ series was included here as we found that the inclusion of diffuse functions improves basis set convergence for the CV correction in fluorine-containing species. Scalar relativistic effects, REL, were accounted for by taking the difference between RHF-UCCSD(T) energies with and without the Douglas-Kroll-Hess relativistic one-electron integrals using the aug-cc-pwCVnZ-DK basis sets.[49] Diagonal

Born-Oppenheimer corrections, DBOC, were computed at CCSD/cc-pVnZ for smaller species or HF/cc-pVnZ for larger species based on computational feasibility. Spin-orbit effects, SO, were not considered as significant for the species used in this work, as indicated in **Table S1**.

All reaction energies were corrected by the zero-point vibrational energies (ZPVE), computed at the highest possible level of theory based on converged minimum geometries at the same level of theory, ensuring that imaginary (negative) frequencies were not present. For smaller species (typically 7 to 8 heavy atoms or less), the CCSD(T)-F12b/cc-pVnZ-F12 methods were used, and for larger species, the double-hybrid and dispersion-corrected density functional method, B2PLYP-D3(BJ), was used with the cc-pVnZ basis sets.[50–53] Anharmonicity corrections (ANH) were computed using second-order vibrational perturbation theory (VPT2), implemented at the CCSD(T)/cc-pVnZ levels for smaller species and at the B2PLYP-D3(BJ)/cc-pVnZ levels for larger species.[54] For species with torsional modes, the corresponding harmonic frequency was replaced and corrected by the one-dimensional hindered-rotor model,[55] with internal rotation potentials evaluated at B2PLYP-D3(BJ)/cc-pVTZ.

CBS limits were estimated using two-point extrapolation forms, with coefficients of 0.46 for DZ-TZ energy extrapolations, 0.69 for TZ-QZ energy extrapolations, 0.93 for QZ-5Z energy extrapolations, 1.20 for 5Z-6Z energy extrapolations, 0.50 for TZ-F12/QZ-F12 energy extrapolations, 0.80 for QZ-F12/5Z-F12 energy extrapolations, and 0.5 for all TZ-QZ and TZ-F12/QZ-F12 frequency, ZPVE, and VPT2-based anharmonicity correction extrapolations.

The thermochemical parameters were fitted to 7-coefficient NASA polynomials[56] in both the CHEMKIN and Cantera formats.[57,58] The computed enthalpies of formation at 0 K for both reference and target species are given in the **Supporting Information** in **Table S1**. Comparisons of the enthalpies of formation at 0 K for the target species with recent literature values is shown in **Table 1**, shown with the level of theory at which the literature values were reported. Overall, excellent agreement is observed for the smaller species, and slightly larger discrepancies for the larger species. We recommend the usage of the present results

11

due to the robustness of the composite quantum chemistry used in this work.

Table 1: Computed $\Delta_f H_{0K}^{\circ}$ and comparisons to literature.

Species	This Work	ATcT V1.202	diet-HEAT[59,60]	diet-HEAT-F12[61]	ANL0[62]	G4[9]	CBH[63]
CF_3	-111.16 ± 0.08	-111.17 ± 0.10	N/A	N/A	-111.19 ± 0.43	N/A	N/A
C_2F_5	-212.75 ± 0.20	N/A	-212.46 ± 0.67	N/A	-212.76 ± 0.43	N/A	N/A
C_2F_6	-318.33 ± 0.40	-318.85 ± 0.19	-318.19 ± 0.76	-319.72 ± 0.67	-318.31 ± 0.43	N/A	N/A
C_3F_7	-311.09 ± 0.39	N/A	N/A	N/A	N/A	-313.33 ± 1.40	N/A
C_3F_8	-415.70 ± 0.48	N/A	N/A	N/A	N/A	-416.22 ± 1.40	-416.78 ± 0.48
C_4F_{10}	-512.52 ± 0.92	N/A	N/A	N/A	N/A	-513.70 ± 1.40	-514.01 ± 0.72

2.3 Pressure-Dependent Rate Constants

Temperature-dependence and pressure-dependence of the phenomenological rate coefficients were modeled by solving the one-dimensional master equation (ME) using *ab initio* based Rice-Ramsperger-Kassel-Marcus (RRKM) theory at the *E*-resolved (microcanonical) level to predict the microscopic rates. To avoid numerical instabilities and low eigenvalue issues, well truncation was implemented by setting a maximum of 10 for the ratio of the dissociation limit to the temperature. Below this threshold, all energy states were assumed to be Boltzmann-populated. A temperature grid ranging from 200−3000 K and a pressure grid ranging from 0.001−100 atm have been used.

2.3.1 Collision Models

The collisional energy transfer behavior for each system were represented by the single exponential down model, parameters for which were drawn by analogy to similar hydrocarbon systems.[64,65] Calculated values of the collisional energy transfer range parameter $\alpha = \langle \Delta E_d \rangle$ were drawn from the classical trajectory simulations of Jasper and used directly in the single exponential down form.[64] Analogies were made by comparison to hydrocarbons with both the same number of heavy atoms ($N_{heavy} = 8$ for C_2F_6, $N_{heavy} = 11$ for C_3F_8, and $N_{heavy} = 14$ for C_4F_{10}) and analogous heavy-atom connectivity. To compute the collision frequencies, Lennard-Jones collision parameters (collision diameter σ and well depth ε) were estimated for the C_2F_6 and C_3F_8 systems with an N_2 bath gas, by direct dynamics. The

12

intermolecular potentials were evaluated at the DF-MP2/aug-cc-pVDZ level for various different sampled orientations, and Lennard-Jones parameters were determined using one-dimensional minimizations within each sampled orientation.[65] For the largest system, C_4F_{10}, falloff behavior of the corresponding reactions is predicted to be minimal, with limited sensitivity of the RRKM/ME calculations to the chosen Lennard-Jones collision model. So, instead of an expensive direct dynamics approach, Lennard-Jones parameters are instead simply estimated by empirical fitting, based on scaling the calculated parameters for C_2F_6 and C_3F_8 by the ratios of Lennard-Jones parameters estimated from the number of heavy atoms.[64] **Table S2** shows the complete set of input parameters for the collision models used in the RRKM/ME calculations, with 95% confidence intervals reported for the Lennard-Jones parameters that were determined by direct dynamics.

2.4 Software

VRC-TST calculations were implemented in the `VaReCoF` program.[66] The `OneDMin` code was used for the estimation of Lennard-Jones parameters.[67] Electronic structure calculations using density functional theory were performed in `Gaussian09` and `Gaussian16`,[68,69] and wavefunction methods were performed in `MOLPRO`,[70–72] as well as the `MRCC` program[73,74] extension to `MOLPRO` for the implementation of coupled-cluster theory with higher order excitations for open-shell species and for CCSDTQ(P) and beyond for closed-shell species. Diagonal Born-Oppenheimer corrections (DBOC) and CCSDT(Q) calculations for closed-shell species were implemented in the `CFOUR` program.[75] The `MESS` program was used for master equation calculations. Subroutines for automating the workflow of composite thermochemistry and master equation kinetics computations were sourced from the `AutoMech` package.[76]

3. Results and Discussion

3.1 Benchmarking $2\,CF_3 \rightleftharpoons C_2F_6$

To gauge the appropriateness of a CASPT2/cc-pVDZ potential for the VRC-TST calculations, various potential corrections as described in **Section 2.1.1** were benchmarked against the chosen standard of the average of spin-splitting approaches with singlet-triplet gaps obtained with both MRCI-F12+Q/aug-cc-pVTZ-F12 and CASPT2-F12/aug-cc-pVTZ-F12. In the shorter range, it is expected that the more rigorous and expensive configuration interaction (CI) energies are more accurate. However, in the long range, the lack of size consistency in truncated CI implementations indicates that the CASPT2 potential may be more accurate.

Furthermore, geometry relaxation effects are neglected in the orientational sampling procedure within the VRC-TST calculation, and the correction to the potential must account for this effect as well. The following describes calculations performed to construct the one-dimensional orientation-independent correction term for the CASPT2/cc-pVDZ potential, as a function only of the radical-radical separation coordinate, R_{CC} [Å].

The geometry relaxation component to the total correction is gauged using the difference between relaxed and rigid CASPT2/cc-pVDZ potentials along the D_{3d} MEP), as shown in **Figure 1** as a function of the radical-radical separation distance, R_{CC}. These corrections are very small due to the strongly non-planar C_{3v} geometry of CF_3 requiring minimal rearrangement as the radicals approach each other. In contrast, with the analogous hydrocarbon reaction $2\,CH_3 \rightleftharpoons C_2H_6$ there is a large rearrangement and geometry relaxation effect arising from the transition from the planar geometry of CH_3 to the sp^3-hybridization in C_2H_6.
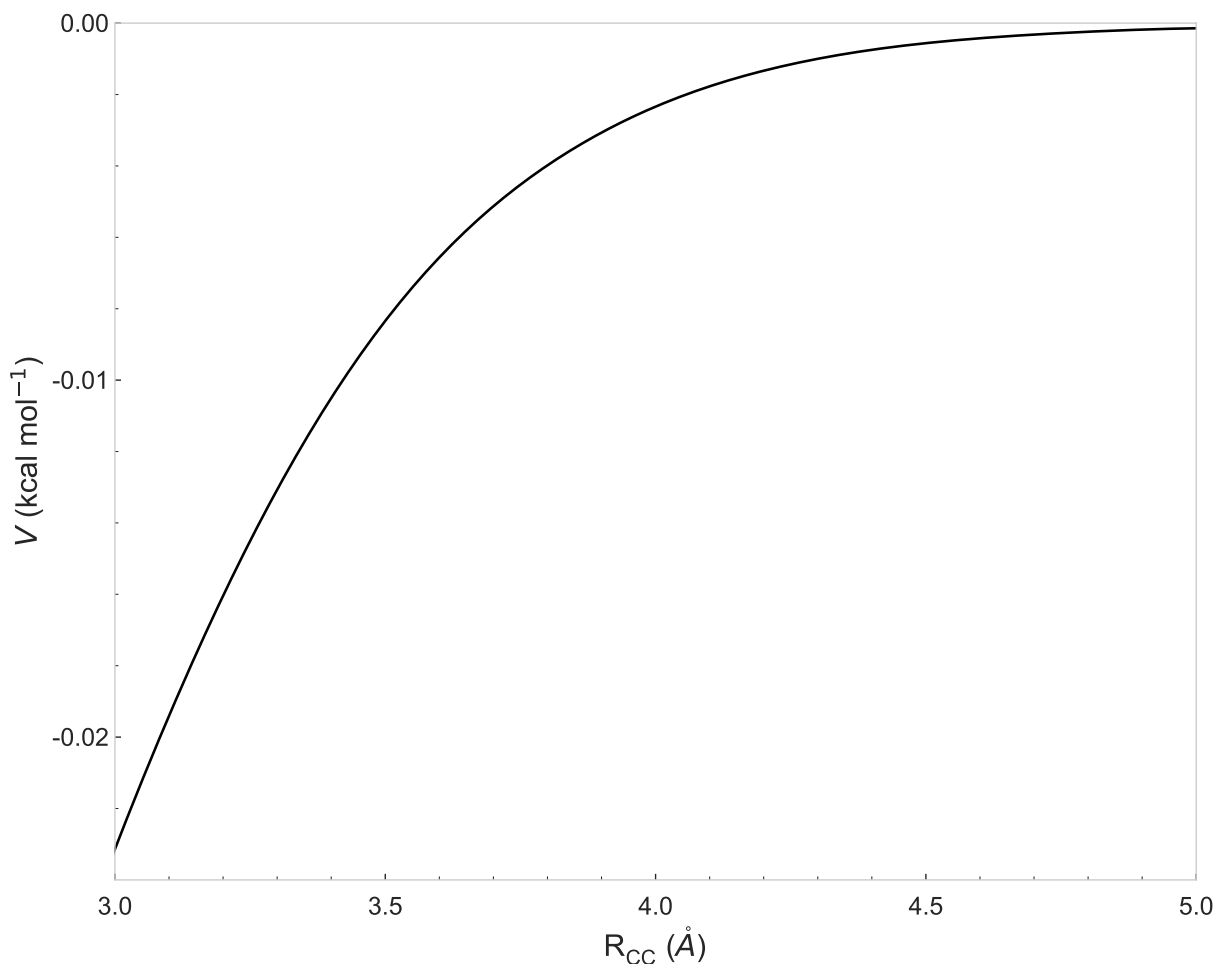
Figure 1: Geometry relaxation component of the correction potential for $CF_3 + CF_3$ association MEP based on relaxed and rigid CASPT2/cc-pVDZ energies.

The correction potential for overcoming method and basis set limitations is given by the difference between the higher level energies obtained for the CASPT2-F12/aug-cc-pVTZ-F12 fully relaxed D_{3d} MEP and the CASPT2/cc-pVDZ energies on the same MEP. The multiple options for this correction potential are plotted along the CASPT2-F12/aug-cc-pVTZ-F12 D_{3d} MEP in **Figure 2a**. The total correction term is given by the sum of the component for geometry relaxation and the component for method and basis set limitations. With respect to the average spin-splitting potential (taken as the reference), the percentage deviations of the other potentials along the MEP are shown in **Figure 2b**, while the correction potential and its percentage relative to the total potential are shown in **Figure 2c**.
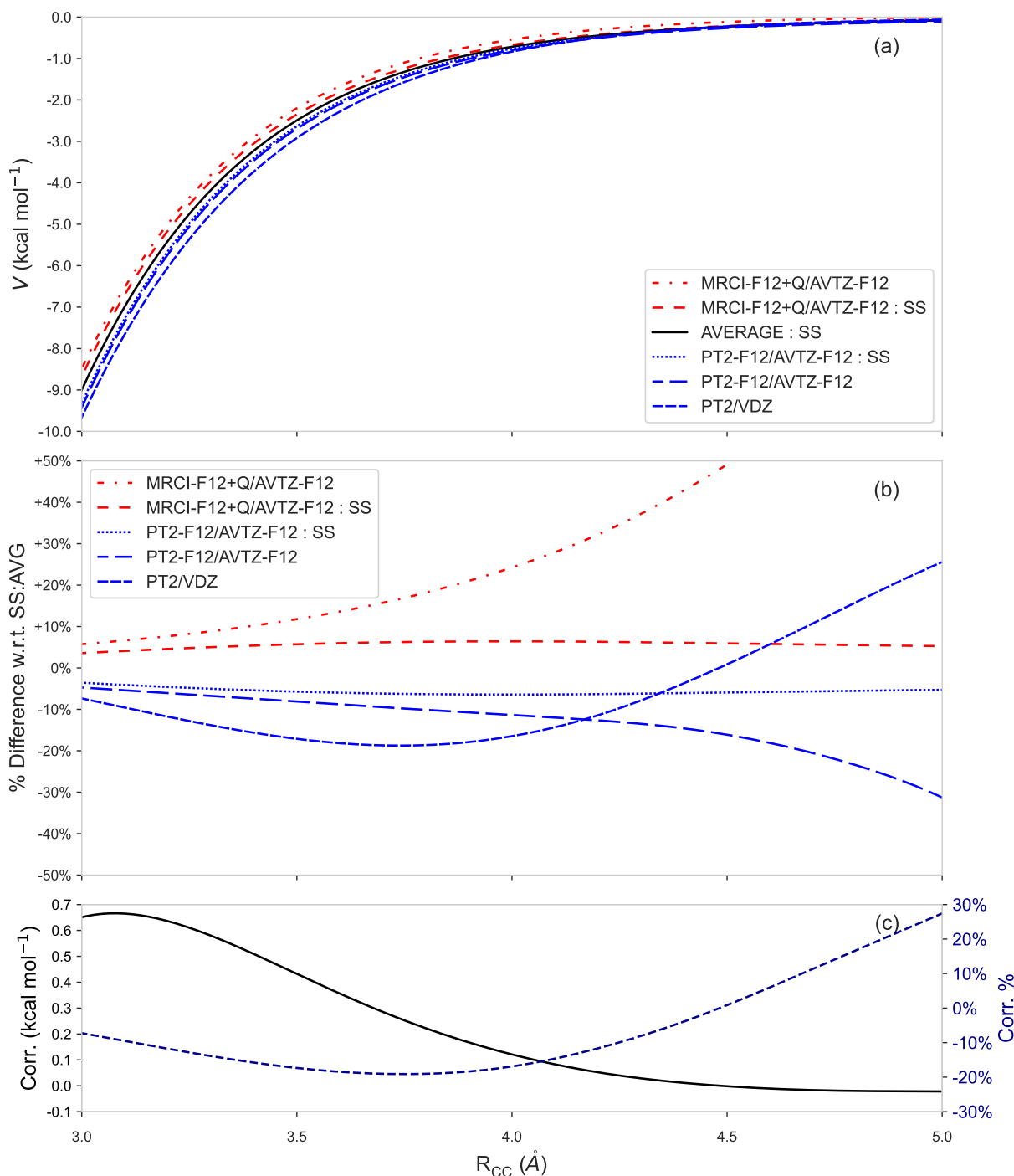
15

Figure 2: **(a)** Various potentials along a D_{3d} $CF_3 + CF_3$ association MEP relaxed at CASPT2-F12/aug-cc-pVTZ-F12, plotted against the coordinate R_{CC} [Å], the radical site separation distance. Shorthand is used for methods and basis sets ("VDZ" is cc-pVDZ, "AVTZ-F12" is aug-cc-pVTZ-F12, and "PT2" is CASPT2), and "SS" refers to spin-splitting approaches. **(b)** Percentage difference of each of the potentials along the D_{3d} $CF_3 + CF_3$ association MEP with respect to (w.r.t.) the average potential calculated by the two spin-splitting approaches. **(c)** Correction potential based on average spin-splitting interaction energies (left) and the percentage of correction potential magnitude relative to total average spin-splitting interaction energy.

16

In the long range, all the spin-splitting potentials are in somewhat good agreement. It can be speculated that both the lack of size consistency and the internal contraction error in the configuration interaction calculations lead to the discrepancy in the MRCI-F12+Q/aug-cc-pVTZ-F12 potential, and it is seen that the spin-splitting approach resolves the issue when the singlet-triplet gap is calculated using the same multireference method. In the shorter range, the potentials computed with the pure CASPT2-F12/aug-cc-pVTZ-F12 calculation and the spin-splitting approach with CASPT2-F12/aug-cc-pVTZ-F12 singlet-triplet gaps do not significantly differ. Similarly, the use of the spin-splitting approach with MRCI-F12+Q/aug-cc-pVTZ-F12 singlet-triplet gaps shows much closer agreement with the pure MRCI-F12+Q/aug-cc-pVTZ-F12 potential, which is likely to be the more accurate of the two multireference approaches at shorter fragment separations. The average of the two spin-splitting approaches is likely to be most accurate overall in the transition state region.

Based on these findings, the use of a CASPT2/cc-pVDZ potential along with the correction based on the average of the spin-splitting approaches, is taken to be the reference method in subsequent potential evaluations for the calculation of high-pressure-limit rate coefficients by VRC-TST. These conclusions are further validated in **Figure 2b** and **Figure 2c**. The small correction potential validates the high-level-corrected CASPT2/cc-pVDZ approach in yielding a high accuracy in the predicted rate coefficients.

To gauge the uncertainty arising from the choice of potential correction term, a simple test was performed. VRC-TST rate coefficients were evaluated with each correction term, and also with no correction term, using a single dividing surface defined by two pivot points on each CF_3 fragment. The pivot points were located approximately 0.5 Å from each face of the radical site along the C_{3v} axis of the CF_3. The point-to-point separation distance was set at approximately 3.5 Å. This corresponds to the optimal canonical transition-state dividing surface between approximately $600-800$ K. The results of this calculation are shown in **Figure 3**, and the trend of the magnitudes of the rate coefficients in the optimal region are in the reverse order of the trend seen in the potentials from **Figure 1**.
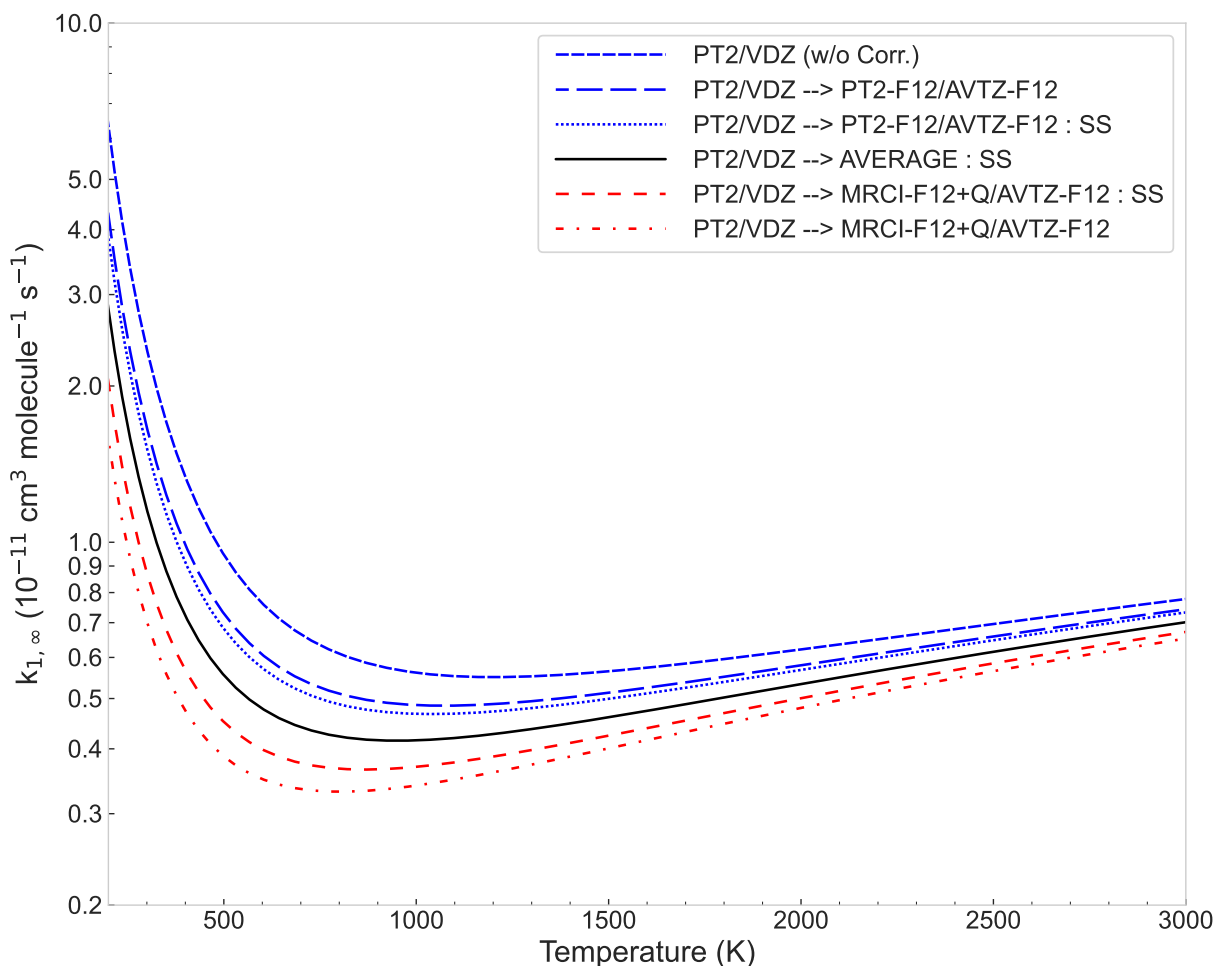
Figure 3: Dynamically-corrected VRC-TST predictions of the high-pressure-limit rate coefficients for $2\,\mathrm{CF_3} \rightleftarrows \mathrm{C_2F_6}$ in the $200-3000$ K temperature range, using various potential correction terms and an optimal canonical transition-state dividing surface in the $600-800$ K region.

The pure CASPT2/cc-pVDZ predictions are too high, and the predictions obtained using the correction factors obtained from MRCI-F12+Q/aug-cc-pVTZ-F12 calculations are too low. Using the correction factors obtained from the spin-splitting approach with singlet-triplet gaps obtained from CASPT2-F12/aug-cc-pVTZ-F12 calculations makes almost no difference with respect to using the corrections obtained from pure CASPT2-F12/aug-cc-pVTZ-F12 calculations. The use of corrections obtained from the spin-splitting approach with MRCI-F12+Q/aug-cc-pVTZ-F12 singlet-triplet gaps gives more intermediary results. Overall, the uncertainty to the choice of potential correction (i.e., a term on top of the pure

18

CASPT2/cc-pVDZ potentials) with respect to the reference spin-splitting average in the $600-800$ K region is approximately on the order of 25%.

The full VRC-TST predictions for the high-pressure limit thermal kinetics of $2\,CF_3 \rightleftharpoons C_2F_6$ can be found in **Figure 4**. The predictions based on two pivot points are more robust, as the positioning of pivot points on either face of the radical fragment gives a superior description of the variational transition states and yields lower rate constants than the predictions based on a single pivot point, illustrating the benefits of constructing a multifaceted dividing surface in providing more accurate results. The present results are also compared with the flexible TST results of Wardlaw and co-workers, which employed a more empirical potential energy surface and were constrained to a reaction coordinate given by the center-of-mass separation distance.[11] These prior calculations agree with the present ones to within about a factor of two.

The contribution of the four faces of the multifaceted dividing surface when using two pivot points follows a trend based on steric and electronic effects. The four faces are termed "front-to-front", "front-to-back" (equivalent to "back-to-front"), and "back-to-back". Here, given the non-planar C_{3v} symmetry of CF_3, the "front" side refers to the face defined by the pivot point located on the side of the radical opposite the fluorines, and the "back" side refers to the face defined by the pivot point located on the same side as the fluorines. The pivot point placement defining the multifaceted dividing surface for $CF_3 + CF_3$ are illustrated as a representative example in **Figure S1**. The front-to-front path, with the two maximum density radical lobes pointing toward each other, is the most energetically favorable approach. Lower steric effects are also expected for this path. At low temperatures, the front-to-front contribution to the total flux is about 60–65%, the front-to-back and back-to-front contributions are roughly 15% each, and the contribution of the back-to-back approaches is already minimal at around 5–10%. At 1000 K, the back-to-front and front-to-back contributions are about 5% each, and the back-to-back contribution is negligible. At 2500 K, the back-to-front and front-to-back contributions decreases to about 2% each.
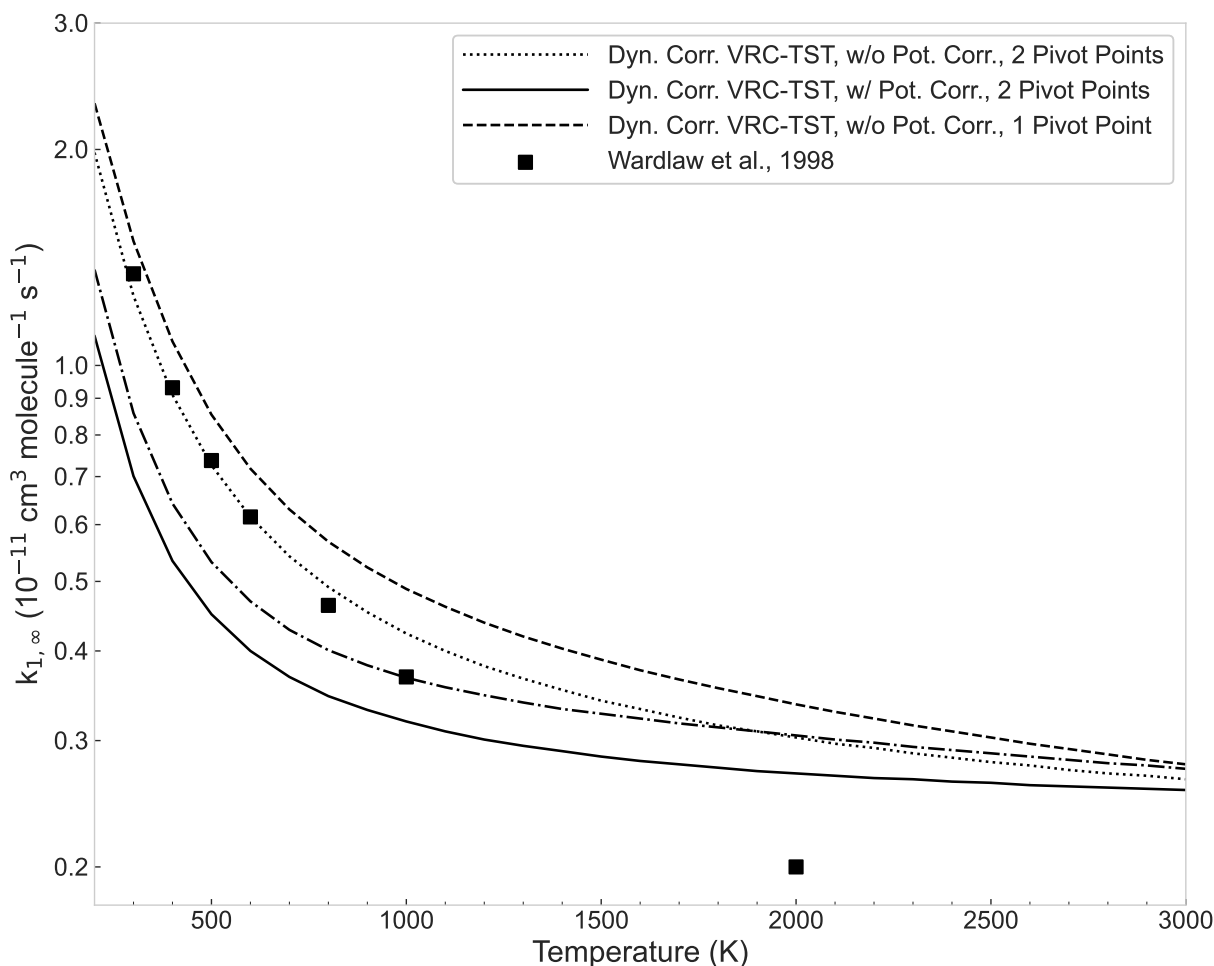
19

Figure 4: Dynamically-corrected VRC-TST predictions of the high-pressure-limit rate coefficients, $k_{1,\infty}$, for $2\,CF_3 \rightleftharpoons C_2F_6$ in the $200-3000$ K temperature range, compared with flexible TST results of Wardlaw and co-workers.[11]

The theoretically predicted pressure-dependent rate constants for $2\,CF_3 \rightleftharpoons C_2F_6$ are plotted in **Figure 5**. Room temperature experimental data are also plotted in this figure.[77–81] Experimental data at higher temperatures involve substantive and likely unreliable pressure extrapolations and are in considerable discord with the present results (more than an order of magnitude).[82–84] Even room-temperature experimental reports vary by about one order of magnitude despite similar experimental conditions. Furthermore, the variation in the experimental results with pressure appears more or less random. The present results are within this range, validating the appropriateness of the chosen scheme to describe the radical-radical

https://doi.org/10.26434/chemrxiv-2024-9m3pc-v3 ORCID: https://orcid.org/0009-0006-8000-0845 Content not peer-reviewed by ChemRxiv. License: CC BY 4.0

interaction potential. At room temperature, the VRC-TST calculation predicts virtually no pressure dependence. In fact, under temperatures of $800-900$ K, the rate constant at 0.001 atm is within approximately a factor of two of the high-pressure limit rate coefficient. Above this temperature, the falloff behavior becomes more significant.
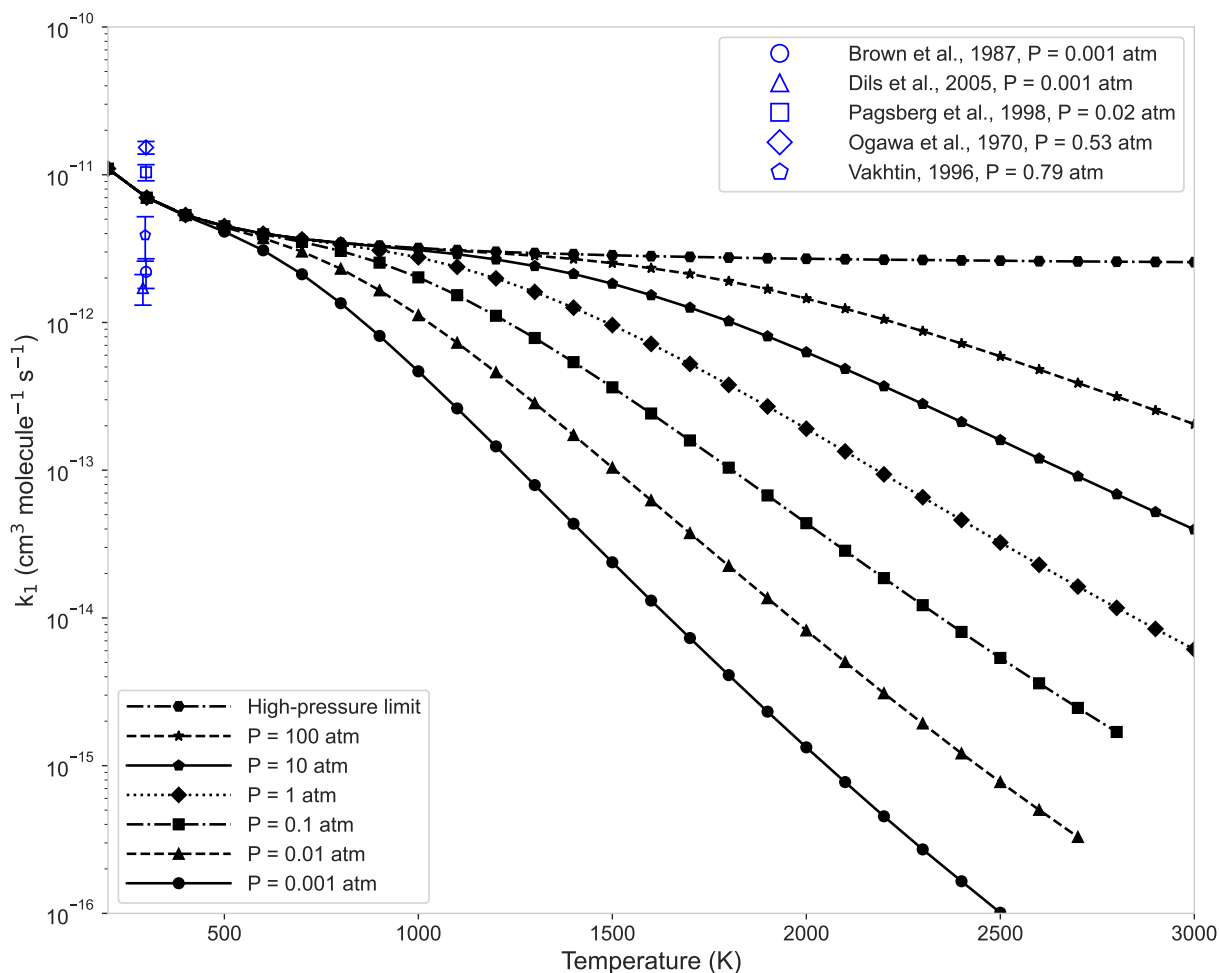

Figure 5: Pressure-dependent rate coefficients $k_1(T, P)$ for $2\,CF_3 \rightleftarrows C_2F_6$ employing N_2 as a bath gas, plotted in the $200-3000$ K temperature range and compared with selected literature data at room temperature.[77-81]

3.2 Size-Dependence of n-C_nF_{2n+1} Radical Association Kinetics

Reactions R2–R4 describing the associations of CF_3 with C_2F_5 and C_3F_7, as well as the self-association of C_2F_5, were treated using the same dynamically-corrected VRC-TST and

21

RRKM/ME approaches as described above. The same correction term for the interaction potential was used as well. This assumption of minimal changes in the interfragment correction potentials, is based on previous precedent in the study of alkyl radical combinations,,[21] as well as minimal changes in the geometry relaxation contribution to the correction term, which was already small to begin with. **Figure S2**, **Figure S3**, and **Figure S4** show the same dependence of the theoretical predictions on correction potential and pivot point treatment for the high-pressure-limit rate coefficients for each remaining case.

To study the size-dependent properties of the n-perfluoroalkyl associations, the high-pressure-limit rate coefficients for the four reactions considered have been plotted together in **Figure 6**. For the self-association reactions, the symmetry factor of 2 has been re-incorporated into the rate coefficients to properly compare the trends as the participating n-perfluoroalkyl chains grow in size. The observed behavior is further explained by the potentials along the highest-possible-symmetry MEPs for each of the cases, shown in **Figure 7** and adjusted by the potential correction constructed as described earlier.

At all temperatures, the self-association reaction of C_2F_5 possesses the lowest rate coefficient. Both steric and electronic effects can contribute to this behavior. Bulky trifluoromethyl groups attached to not one, but both fragments involved, generate comparatively unfavorable steric effects along the reaction coordinate, and the potential along the MEP is also seen to be less attractive than for all the other cases. At higher temperatures, the self-association reaction of CF_3 possesses a consistently higher rate coefficient than both of the cross-association reactions. Given that the optimal transition-state dividing surfaces at these temperatures are located at shorter separation distances, the observed trend can be explained by steric effects. At lower temperatures, the optimal transition-state dividing surfaces are located at further separations. Thus, the higher coefficients for the cross-association reactions can likely be justified by their more attractive potentials along their MEPs. As temperatures rise into more intermediate levels, a combination of the steric and electronic effects described above appear to determine the size-dependent behavior of the association rate constants.

22

Figure S5 shows the predicted pressure-dependent rate constants at selected temperatures for the $CF_3 + C_2F_5 \rightleftharpoons C_3F_8$. The falloff effect for this reaction was found to be diminished in comparison to $CF_3 + CF_3 \rightleftharpoons C_2F_6$, as expected with the increase in size. The pressure dependence for the $CF_3 + C_3F_7$ reaction is somewhat more complex, as the bimolecular reaction to form two C_2F_5 radicals competes with stabilization within the C_4F_{10} well. **Figure S6** and **Figure S7** show the predicted pressure-dependent rate constants for the two stabilization channels, $CF_3 + C_3F_7 \rightleftharpoons C_4F_{10}$ and $2\,C_2F_5 \rightleftharpoons C_4F_{10}$. The falloff effect for these two reactions is also diminished.
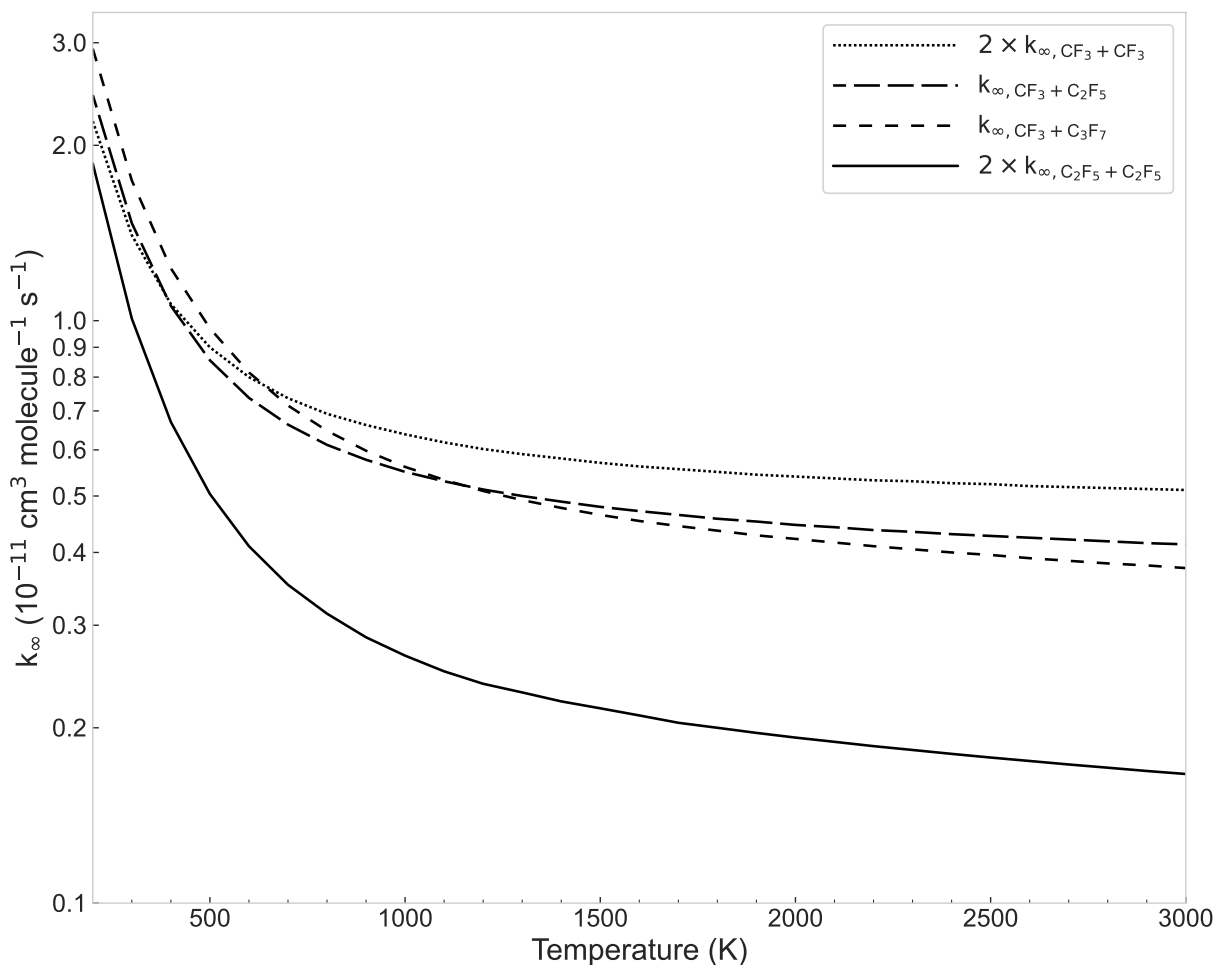

Figure 6: Size-dependent trends in the dynamically-corrected VRC-TST predictions for all considered reactions.

The reaction over the well, $CF_3 + C_3F_7 \rightleftharpoons 2\,C_2F_5$, was also studied. In the high-pressure limit, the rate coefficients for this reaction vanish ($k_{5,\infty} = 0$), and the rate constants at pressures between 0.001 atm and 100 atm have been plotted in **Figure 8**. The reaction enthalpy of $CF_3 + C_3F_7 \rightleftharpoons 2\,C_2F_5$ is computed to be -3.26 kcal mol^{-1}. In accordance with the intuition associated with the greater exothermicity of $CF_3 + C_3F_7 \rightleftharpoons C_4F_{10}$ compared to $2\,C_2F_5 \rightleftharpoons C_4F_{10}$, which in other words refers to greater bond dissociation energies at terminal $C-C$ bonds, R3 outcompetes R4 and equilibrium favors the forward direction of $CF_3 + C_3F_7 \rightleftharpoons 2\,C_2F_5$.
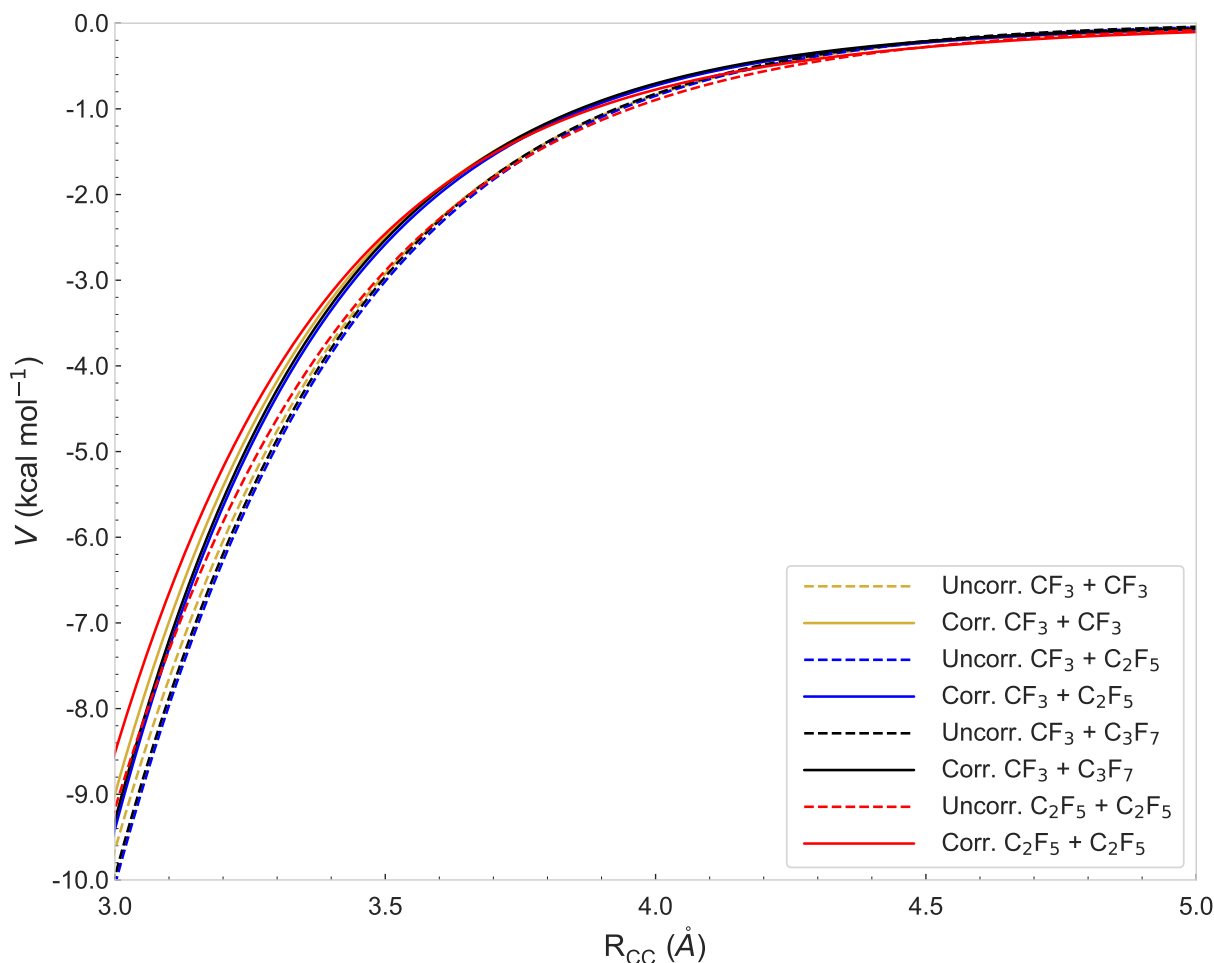

Figure 7: Corrected and uncorrected potentials along the highest-possible-symmetry MEPs for all considered reactions, plotted against the coordinate R_{CC} [Å], the radical site separation distance.

It is worth noting that the geometric mean rule (as described for alkyl combination reactions[21]) can be used to reasonably predict rate coefficients for larger radical combinations. For example, the rate coefficients for the self-combination of C_3F_7 may be predicted on the basis of the rate coefficients for $CF_3 + CF_3$ and $CF_3 + C_3F_7$.
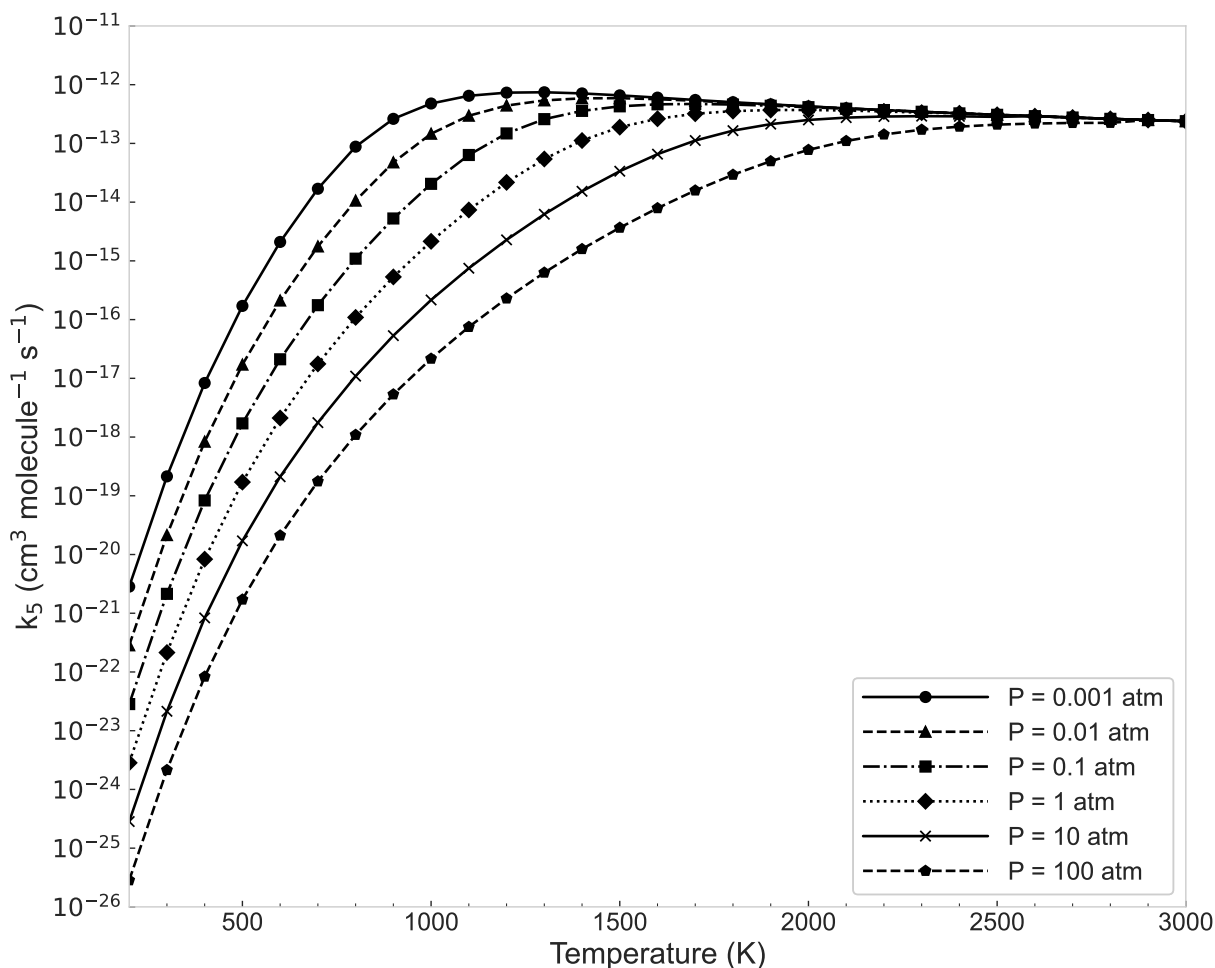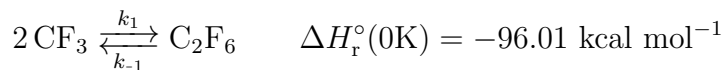

Figure 8: Pressure-dependent rate coefficients k_5 for the well-skipping reaction $CF_3 + C_3F_7 \rightleftharpoons 2\,C_2F_5$ employing N_2 as a bath gas, plotted in the $200-3000$ K temperature range.

4. Conclusions

Comprehensive kinetics and reaction thermochemistry have been predicted for the four radical association reactions forming the $C_2 - C_4$ n-perfluoroalkanes, as well as the bimolecular well-skipping reaction over the C_4F_{10} well. A high-level correction potential for CASPT2/cc-pVDZ direct dynamics potential evaluations in VRC-TST has been developed for $CF_3 + CF_3$ based on spin-splitting approaches, and implemented in the calculation of high-pressure-limit rate coefficients. ANL0/ANL1-like composite quantum chemistry methodologies have been used to compute enthalpies of formation for the target species using the CBH0, CBH1, CBH2, and CBH3 rungs of the error-cancelling reaction schemes. This combination of ANL schemes and CBH schemes provide low uncertainty in the computed enthalpies of formation.

Computed enthalpies of reaction and estimates of transport parameters and collision models have been used with *ab initio*-based RRKM theory and the one-dimensional master equation to obtain the microscopic rates, high-pressure-limit canonical rate coefficients, and pressure-dependent kinetics. Both high-pressure-limit and pressure-dependent kinetics are reported in the form of modified Arrhenius expressions that are reasonably well-fitted and are designed for logarithmic interpolation. Computed thermochemical parameters for the perfluoroalkyl radicals and perfluoroalkanes considered in this work have been also been fitted to 7-coefficient NASA polynomials and reported in standardized formats.

Below, the enthalpies of reaction at 0 K and the high-pressure limit fitted rate expressions (valid between 200 K and 3000 K) are reported for each of the reactions studied in this work. We expect these expressions to prove useful in future modeling studies. The size-dependent trends of the radical combinations are affected by both steric and electronic phenomena, and these considerations can be implemented heuristically in estimate the rates of radical combinations for larger species. With these considerations in mind, the reported rate expressions should be useful in rule-based extrapolations to larger molecules (e.g., geometric mean rule), especially in the high pressure limit.
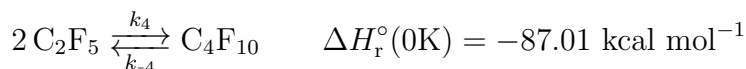
https://doi.org/10.26434/chemrxiv-2024-9m3pc-v3 ORCID: https://orcid.org/0009-0006-8000-0845 Content not peer-reviewed by ChemRxiv. **License:** CC BY 4.0

$$2\,\mathrm{CF_3} \underset{k_{-1}}{\overset{k_1}{\rightleftharpoons}} \mathrm{C_2F_6} \qquad \Delta H_\mathrm{r}^\circ(0\mathrm{K}) = -96.01 \text{ kcal mol}^{-1}$$

$$k_{1,\infty}(T) = (3.85 \times 10^{-12})T^{-0.07} \exp\left(281/T\right)$$

$$\mathrm{CF_3} + \mathrm{C_2F_5} \underset{k_{-2}}{\overset{k_2}{\rightleftharpoons}} \mathrm{C_3F_8} \qquad \Delta H_\mathrm{r}^\circ(0\mathrm{K}) = -91.78 \text{ kcal mol}^{-1}$$

$$k_{2,\infty}(T) = (1.15 \times 10^{-11})T^{-0.15} \exp\left(307/T\right)$$

$$\mathrm{CF_3} + \mathrm{C_3F_7} \underset{k_{-3}}{\overset{k_3}{\rightleftharpoons}} \mathrm{C_4F_{10}} \qquad \Delta H_\mathrm{r}^\circ(0\mathrm{K}) = -90.36 \text{ kcal mol}^{-1}$$

$$k_{3,\infty}(T) = (3.94 \times 10^{-11})T^{-0.31} \exp\left(275/T\right)$$

$$2\,\mathrm{C_2F_5} \underset{k_{-4}}{\overset{k_4}{\rightleftharpoons}} \mathrm{C_4F_{10}} \qquad \Delta H_\mathrm{r}^\circ(0\mathrm{K}) = -87.01 \text{ kcal mol}^{-1}$$

$$k_{4,\infty}(T) = (1.49 \times 10^{-11})T^{-0.38} \exp\left(315/T\right)$$

$$\mathrm{CF_3} + \mathrm{C_3F_7} \underset{k_{-5}}{\overset{k_5}{\rightleftharpoons}} 2\,\mathrm{C_2F_5} \qquad \Delta H_\mathrm{r}^\circ(0\mathrm{K}) = -3.26 \text{ kcal mol}^{-1}$$

5. Acknowledgements

Workforce Development for Teachers and Scientists (WDTS) under the Science Undergraduate Laboratory Internships (SULI) program. The authors declare no competing interests.

6. Data Availability

Mechanism files have been provided in the `CHEMKIN` ("chemkin.inp") and `Cantera` ("cantera.yaml") formats, including both kinetics and thermochemistry. Documents with supplementary tables ("Tables.pdf") and supplementary figures ("Figures.pdf") have been provided. A spreadsheet ("kTP_Tables.xlsx") containing pressure/temperature rate coefficient tables is provided. Finally, `MESS` input files for the calculation of species partition functions and reaction kinetics have been provided, in which the computed molecular geometries, rovibrational data, and other necessary information are given.

References

(1) Sunderland, E. M.; Hu, X. C.; Dassuncao, C.; Tokranov, A. K.; Wagner, C. C.; Allen, J. G. A review of the pathways of human exposure to poly- and perfluoroalkyl substances (PFASs) and present understanding of health effects. *J. Expo. Sci. Environ. Epidemiol.* **2019**, *29*, 131–147.

(2) Olsen, G. W.; Church, T. R.; Miller, J. P.; Burris, J. M.; Hansen, K. J.; Lundberg, J. K.; Armitage, J. B.; Herron, R. M.; Medhdizadehkashi, Z.; Nobiletti, J. B. et al. Perfluorooctanesulfonate and other fluorochemicals in the serum of American Red Cross adult blood donors. *Environ. Health Perspect.* **2003**, *111*, 1892–1901.

(3) Kannan, K.; Choi, J.-W.; Iseki, N.; Senthilkumar, K.; Kim, D. H.; Masunaga, S.; Giesy, J. P. Concentrations of perfluorinated acids in livers of birds from Japan and Korea. *Chemosphere* **2002**, *49*, 224–231.

(4) Kannan, K.; Corsolini, S.; Falandysz, J.; Fillmann, G.; Kumar, K. S.; Loganathan, B. G.; Mohd, M. A.; Olivero, J.; Wouwe, N. V.; Yang, J. H. et al. Perfluorooctanesulfonate and Related Fluorochemicals in Human Blood from Several Countries. *Environ. Sci. Technol.* **2004**, *38,*, 4489–4495.

(5) Li, Y.; Fletcher, T.; Mucs, D.; Scott, K.; Lindh, C. H.; Tallving, P.; Jakobsson, K. Half-lives of PFOS, PFHxS and PFOA after end of exposure to contaminated drinking water. *Occup. Environ. Med.* **2018**, *75*, 46–51.

(6) Shields, E. P.; Krug, J. D.; Roberson, W. R.; Jackson, S. R.; Smeltz, M. G.; Allen, M. R.; Burnette, R. P.; Nash, J. T.; Virtaranta, L.; Preston, W. et al. Pilot-Scale Thermal Destruction of Per- and Polyfluoroalkyl Substances in a Legacy Aqueous Film Forming Foam. *ACS EST Engg.* **2023**, *3*, 1308–1317.

(7) Altarawneh, M.; Almatarneh, M. H.; Dlugogorski, B. Z. Thermal decomposition of

perfluorinated carboxylic acids: Kinetic model and theoretical requirements for PFAS incineration. *Chemosphere* **2022**, *286*, 131685.

(8) Altarawneh, M. A chemical kinetic model for the decomposition of perfluorinated sulfonic acids. *Chemosphere* **2021**, *263*, 128256.

(9) Ram, H.; Sadej, T. P.; Murphy, C. C.; Mallo, T. J.; Westmoreland, P. R. Thermochemistry of Species in Gas-Phase Thermal Oxidation of C_2 to C_8 Perfluorinated Carboxylic Acids. *J. Phys. Chem. A* **2024**, *128*, 1313–1326.

(10) Ram, H.; DePompa, C. M.; Westmoreland, P. R. Thermochemistry of Species in Gas-Phase Thermal Oxidation of C_2 to C_8 Perfluorinated Sulfonic Acids with Extrapolation to C_{16}. *J. Phys. Chem. A* **2024**, *128*, 3387–3395.

(11) Pesa, M.; Pilling, M. J.; Robertson, S. H.; Wardlaw, D. M. Application of the Canonical Flexible Transition State Theory to CH3, CF3, and CCl3 Recombination Reactions. *J. Phys. Chem. A* **1998**, *102*, 8526–8536.

(12) Klippenstein, S. J. From theoretical reaction dynamics to chemical modeling of combustion. *Proc. Combust. Inst.* **2017**, *36*, 77–111.

(13) Miller, W. H.; Handy, N. C.; Adams, J. E. Reaction path Hamiltonian for polyatomic molecules. *J. Chem. Phys.* **1980**, *72*, 99–112.

(14) Wardlaw, D. M.; Marcus, R. A. RRKM reaction rate theory for transition states of any looseness. *Chem. Phys. Lett.* **1984**, *110*, 230–234.

(15) Wardlaw, D. M.; Marcus, R. A. Unimolecular reaction rate theory for transition states of partial looseness. II. Implementation and analysis with applications to NO_2 and C_2H_6 dissociations. *J. Chem. Phys.* **1985**, *83*, 3462–3480.

(16) Truhlar, D. G.; Garrett, B. C.; Klippenstein, S. J. Current Status of Transition-State Theory. *J. Phys. Chem.* **1996**, *100*, 12771–12800.

(17) Klippenstein, S. J. Variational Optimizations in the Rice-Ramsberger-Kassel-Marcus Theory Calculations for Unimolecular Dissociations with No Reverse Barrier. *J. Chem. Phys.* **1992**, *96*, 367–371.

(18) Georgievskii, Y.; Klippenstein, S. J. Variable Reaction Coordinate Transition State Theory: Analytic Results and Application to the $C_2H_3+H \rightarrow C_2H_4$ Reaction. *J. Chem. Phys.* **2003**, *118*, 5442–5455.

(19) Georgievskii, Y.; Klippenstein, S. J. Transition State Theory for Multichannel Addition Reactions: Multifaceted Dividing Surfaces. *J. Phys. Chem. A* **2003**, *107*, 9776–9781.

(20) Harding, L. B.; Georgievskii, Y.; Klippenstein, S. J. Predictive Theory for Hydrogen Atom-Hydrocarbon Radical Association Kinetics. *J. Phys. Chem. A* **2005**, *109*, 4646–4656.

(21) Klippenstein, S. J.; Georgievskii, Y.; Harding, L. B. Predictive theory for the combination kinetics of two alkyl radicals. *Phys. Chem. Chem. Phys.* **2006**, *8*, 1133–1147.

(22) Werner, H.-J. Third-order multireference perturbation theory The CASPT3 method. *Mol. Phys.* **1996**, *89*, 645–661.

(23) Klippenstein, S. J.; Elliott, S. N. OH Roaming during the Ozonolysis of α-Pinene: A New Route to Highly Oxygenated Molecules? *J. Phys. Chem. A* **2023**, *127*, 10647–10662.

(24) Shiozaki, T.; Werner, H.-J. Second-order multireference perturbation theory with explicit correlation: CASPT2-F12. *J. Chem. Phys.* **2010**, *133*, 141103.

(25) Peterson, K. A.; Adler, T. B.; Werner, H.-J. Systematically convergent basis sets for explicitly correlated wavefunctions: The atoms H, He, B-Ne, and Al-Ar. *J. Chem. Phys.* **2008**, *128*, 084102.

(26) Kendall, R. A.; Dunning, T. H., Jr.; Harrison, R. J. Electron affinities of the firstâĂŘrow

atoms revisited. Systematic basis sets and wave functions. *J. Chem. Phys.* **1992**, *96*, 6796–6806.

(27) Sylvetsky, N.; Kesharwani, M. K.; Martin, J. M. L. The aug-cc-pVnZ-F12 basis set family: Correlation consistent basis sets for explicitly correlated benchmark calculations on anions and noncovalent complexes. *J. Chem. Phys.* **2017**, *147*, 134106.

(28) Werner, H.-J.; Knowles, P. J. An efficient internally contracted multiconfigurationâĂŞreference configuration interaction method. *J. Chem. Phys.* **1988**, *89*, 5803–5814.

(29) Knowles, P. J.; Werner, H.-J. An efficient method for the evaluation of coupling coefficients in configuration interaction calculations. *Chem. Phys. Lett.* **1988**, *145*, 514–522.

(30) Shiozako, T.; Knizia, G.; Werner, H.-J. Explicitly correlated multireference configuration interaction: MRCI-F12. *J. Chem. Phys.* **2011**, *134*, 034113.

(31) Shiozako, T.; Werner, H.-J. Explicitly correlated multireference configuration interaction with multiple reference functions: Avoided crossings and conical intersections. *J. Chem. Phys.* **2011**, *134*, 184104.

(32) Shiozako, T.; Werner, H.-J. Multireference explicitly correlated F12 theories. *Mol. Phys.* **2013**, *111*, 607–630.

(33) Goldsmith, C. F.; Harding, L. B.; Georgievskii, Y.; Miller, J. A.; Klippenstein, S. J. Temperature and Pressure-Dependent Rate Coefficients for the Reaction of Vinyl Radical with Molecular Oxygen. *J. Phys. Chem. A* **2015**, *119*, 7766–7779.

(34) Hampel, C.; Peterson, K. A.; Werner, H.-J. A comparison of the efficiency and accuracy of the quadratic configuration interaction (QCISD), coupled cluster (CCSD), and Brueckner coupled cluster (BCCD) methods. *Chem. Phys. Lett.* **1992**, *190*, 1–12.

(35) Adler, T. B.; Knizia, G.; Werner, H.-J. A simple and efficient CCSD(T)-F12 approximation. *J. Chem. Phys.* **2007**, *127*, 221106.

(36) Knizia, G.; Adler, T. B.; Werner, H.-J. Simplified CCSD(T)-F12 methods: Theory and benchmarks. *J. Chem. Phys.* **2009**, *130*, 054104.

(37) Celani, P.; Werner, H.-J. Multireference perturbation theory for large restricted and selected active space reference wave functions. *J. Chem. Phys.* **2000**, *112*, 5546–5557.

(38) Georgievskii, Y.; Klippenstein, S. J. Long-range transition state theory. *J. Chem. Phys.* **2005**, *122*, 194103.

(39) Ramabhadran, R. O.; Raghavachari, K. Theoretical Thermochemistry for Organic Molecules: Development of the Generalized Connectivity-Based Hierarchy. *J. Chem. Theory Comput.* **2011**, *7*, 2094–2103.

(40) Elliott, S. N.; Keceli, M.; Ghosh, M. K.; Somers, K. P.; Curran, H. J.; Klippenstein, S. J. High-Accuracy Heats of Formation for Alkane Oxidation: From Small to Large via the Automated CBH-ANL Method. *J. Phys. Chem. A* **2023**, *127*, 1512–1531.

(41) Wheeler, S. E.; Houk, K. N.; v. R. Schleyer, P.; Allen, W. D. A Hierarchy of Homodesmotic Reactions for Thermochemistry. *J. Am. Chem. Soc.* **2009**, *131*, 2547–2560.

(42) Ruscic, B.; Pinzon, R. E.; Morton, M. L.; von Laszevski, G.; Bittner, S. J.; Nijsure, S. G.; Amin, K. A.; Minkoff, M.; Wagner, A. F. Introduction to Active Thermochemical Tables: Several âĂIJKeyâĂİ Enthalpies of Formation Revisited. *J. Phys. Chem. A* **2004**, *108*, 9979–9997.

(43) Ruscic, B.; Pinzon, R. E.; von Laszevski, G.; Kodeboyina, D.; Burcat, A.; Leahy, D.; Montoy, D.; Wagner, A. F. Active Thermochemical Tables: thermochemistry for the 21st century. *J. Phys.: Conf. Ser.* **2005**, *16*, 561–570.

(44) Ruscic, B.; Bross, D. H. Active Thermochemical Tables (ATcT); Argonne National Laboratory. https://atct.anl.gov (accessed July 1, 2024).

(45) Klippenstein, S. J.; Harding, L. B.; Ruscic, B. Ab Initio Computations and Active Thermochemical Tables Hand in Hand: Heats of Formation of Core Combustion Species. *J. Phys. Chem. A* **2017**, *121*, 6580–6602.

(46) Kallay, M.; Surjan, P. R. Higher excitations in coupled-cluster theory. *J. Chem. Phys.* **2001**, *115*, 2945–2954.

(47) Kallay, M.; Gauss, J. Approximate treatment of higher excitations in coupled-cluster theory. *J. Chem. Phys.* **2005**, *123*, 214105.

(48) Peterson, K. A.; Dunning, T. H., Jr. Accurate correlation consistent basis sets for molecular coreâĂŞvalence correlation effects: The second row atoms AlâĂŞAr, and the first row atoms BâĂŞNe revisited. *J. Chem. Phys.* **2002**, *117*, 10548–10560.

(49) de Jong, W. A.; Harrison, R. J.; Dixon, D. A. Parallel DouglasâĂŞKroll energy and gradients in NWChem: Estimating scalar relativistic effects using DouglasâĂŞKroll contracted basis sets. *J. Chem. Phys.* **2001**, *114*, 48–53.

(50) Grimme, S. Semiempirical hybrid density functional with perturbative second-order correlation. *J. Chem. Phys.* **2006**, *124*, 034108.

(51) Goerigk, L.; Grimme, S. Efficient and Accurate Double-Hybrid-Meta-GGA Density Functionals-Evaluation with the Extended GMTKN30 Database for General Main Group Thermochemistry, Kinetics, and Noncovalent Interactions. *J. Chem. Theory Comput.* **2011**, *7*, 291–309.

(52) Grimme, S.; Goerigk, L.; Ehrlich, S. Effect of the damping function in dispersion corrected density functional theory. *J. Comp. Chem.* **2011**, *32*, 1456–1465.

(53) Grimme, S.; Antony, J.; Ehrlich, S.; Krieg, H. A consistent and accurate ab initio parametrization of density functional dispersion correction (DFT-D) for the 94 elements H-Pu. *J. Chem. Phys.* **2010**, *132*, 154104.

(54) Bloino, J.; Biczysko, M.; Barone, V. General Perturbative Approach for Spectroscopy, Thermodynamics, and Kinetics: Methodological Background and Benchmark Studies. *J. Chem. Theory Comput.* **2012**, *8*, 1015–1036.

(55) Pfaendtner, J.; Yu, X.; Broadbelt, L. J. The 1-D hindered rotor approximation. *Theor. Chem. Acc.* **2007**, *118*, 881–898.

(56) Gordon, S.; McBride, B. J. Computer Program for Calculation of Complex Chemical Equilibrium Composition, Rocket Performance, Incident and Reflected Shocks and Chapman-Jouguet Detonations, Technical Report NASA-SP-273. *NASA* **1976**, http://hdl.handle.net/2060/19780009781 (accessed July 1, 2024).

(57) Ansys Chemkin-Pro Chemistry Simulation Software. https://www.ansys.com/products/fluids/ansys–chemkin–pro (accessed July 1, 2024).

(58) Goodwin, D. G.; Moffat, H. K.; Schoegl, I.; Speth, R. L.; Weber, B. W. Cantera, Version 3.0.0.: An object-oriented software toolkit for chemical kinetics, thermodynamics, and transport processes. https://www.cantera.org (accessed July 1, 2024).

(59) Ganyecz, A.; Kallay, M.; Csontos, J. Accurate Theoretical Thermochemistry for Fluoroethyl Radicals. *J. Phys. Chem. A* **2017**, *121*, 1153–1162.

(60) Nagy, B.; Csontos, B.; Csontos, J.; SzakAcs, P.; Kallay, M. High-Accuracy Theoretical Thermochemistry of Fluoroethanes. *J. Phys. Chem. A* **2014**, *118*, 4824–4836.

(61) Ganyecz, A.; Kallay, M.; Csontos, J. High Accuracy Quantum Chemical and Thermochemical Network Data for the Heats of Formation of Fluorinated and Chlorinated Methanes and Ethanes. *J. Phys. Chem. A* **2018**, *122*, 5993–6006.

(62) Sharma, S.; Abeywardane, K.; Goldsmith, C. F. Theory-Based Mechanism for Fluo-

romethane Combustion I: Thermochemistry and Abstraction Reactions. *J. Phys. Chem. A* **2023**, *127*, 1499–1511.

(63) Abeywardane, K.; Goldsmith, C. F. Accurate Enthalpies of Formation for PFAS from First-Principles: Combining Different Levels of Theory in a Generalized Thermochemical Hierarchy. *ACS Phys. Chem. Au* **2024**, *4*, 247–258.

(64) Jasper, A. W. âĂIJThird-bodyâĂİ collision parameters for hydrocarbons, alcohols, and hydroperoxides and an effective internal rotor approach for estimating them. *Int. J. Chem. Kinet.* **2020**, *52*, 387–402.

(65) Jasper, A. W.; Miller, J. A. Lennard-Jones parameters for combustion and chemical kinetics modeling from full-dimensional intermolecular potentials. *Combust. Flame* **2014**, *161*, 101–110.

(66) Georgievskii, Y.; Harding, L. B.; Klippenstein, S. J. VaReCoF 2017.05.19.

(67) Jasper, A. W.; Miller, J. A. OneDMin, October 2023.

(68) Frisch, M. J.; Trucks, G. W.; Schlegel, H. B.; Scuseria, G. E.; Robb, M. A.; Cheeseman, J. R.; Scalmani, G.; Barone, V.; Petersson, G. A.; Nakatsuji, H. et al. Gaussian 09 Revision A.02. 2016; Gaussian Inc. Wallingford CT.

(69) Frisch, M. J.; Trucks, G. W.; Schlegel, H. B.; Scuseria, G. E.; Robb, M. A.; Cheeseman, J. R.; Scalmani, G.; Barone, V.; Petersson, G. A.; Nakatsuji, H. et al. Gaussian 16 Revision A.03. 2016; Gaussian Inc. Wallingford CT.

(70) Werner, H.-J.; Knowles, P. J.; Knizia, G.; Manby, F. R.; Schutz, M. Molpro: a general-purpose quantum chemistry program package. *Wiley Interdiscip. Rev. Comput. Mol. Sci.* **2012**, *2*, 242–253.

(71) Werner, H.-J.; Knowles, P. J.; Manby, F. R.; Black, J. A.; Doll, K.; HeÃ§elmann, A.;

Kats, D.; KÃűhn, A.; Korona, T.; Kreplin, D. A. et al. The Molpro quantum chemistry package. *J. Chem. Phys.* **2020**, *152*, 144107.

(72) Werner, H.-J.; Knowles, P. J.; Celani, P.; GyÃűrffy, W.; Hesselmann, A.; Kats, D.; Knizia, G.; KÃűhn, A.; Korona, T.; Kreplin, D. et al. MOLPRO, 2021.2 , a package of ab initio programs. https://www.molpro.net (accessed July 1, 2024).

(73) Kallay, M.; Nagy, P. R.; Mester, D.; Rolik, Z.; Samu, G.; Csontos, J.; CsÃşka, J.; SzabÃş, P. B.; Gyevi-Nagy, L.; HÃĺgely, B. et al. The MRCC program system: Accurate quantum chemistry from water to proteins. *J. Chem. Phys.* **2020**, *152*, 074107.

(74) Kallay, M.; Nagy, P. R.; Mester, D.; Gyevi-Nagy, L.; CsÃşka, J.; SzabÃş, P. B.; Rolik, Z.; Samu, G.; Csontos, J.; HÃĺgely, B. et al. MRCC, a quantum chemical program suite. https://www.mrcc.hu/ (accessed July 1, 2024).

(75) Stanton, J. F.; Gauss, J.; Cheng, L.; Harding, M. E.; Matthews, D. A.; Szalay, P. G. CFOUR, Coupled-Cluster techniques for Computational Chemistry, a quantum-chemical program package. With contributions from A. Asthana, A.A. Auer, R.J. Bartlett, U. Benedikt, C. Berger, D.E. Bernholdt, S. Blaschke, Y. J. Bomble, S. Burger, O. Christiansen, D. Datta, F. Engel, R. Faber, J. Greiner, M. Heckert,O. Heun, M. Hilgenberg, C. Huber, T.-C. Jagau, D. Jonsson, J. Jusélius, T. Kirsch, M.-P. Kitsaras, K. Klein, G.M. Kopper, W.J. Lauderdale, F. Lipparini, J. Liu, T. Metzroth, L. Monzel, L.A. Mück, D.P. O'Neill, T. Nottoli, J. Oswald, D.R. Price, E. Prochnow, C. Puzzarini, K. Ruud, F. Schiffmann, W. Schwalbach, C. Simmons, S. Stopkowicz, A. Tajti, T. Uhlířová, J. Vázquez, F. Wang, J.D. Watts, P. Yergün. C. Zhang, X. Zheng, and the integral packages MOLECULE (J. Almlöf and P.R. Taylor), PROPS (P.R. Taylor), ABACUS (T. Helgaker, H.J. Aa. Jensen, P. Jørgensen, and J. Olsen), and ECP routines by A. V. Mitin and C. van Wüllen. For the current version, see http://www.cfour.de.

(76) Elliot, S. N.; Kevin B. Moore, D. R. M.; Mulvihill, C. R.; Harding, L. B.;

Georgievskii, Y.; Jasper, A. W.; Copan, A. V.; Maffei, L. P.; Cavallotti, C. A.; Keceli, M. et al. AutoMech: Large-Scale Automated Mechanism Modeling, v0.1.2. http://tcg.cse.anl.gov/papr/codes/automech.html (accessed July 1, 2024).

(77) Ogawa, T.; Carlson, G. A.; Pimentel, G. C. Reaction Rate of Trifluoromethyl Radicals by Rapid Scan Infrared Spectroscopy. *J. Phys. Chem.* **1970**, *74*, 2090–2095.

(78) Brown, C. E.; Orlando, J. J.; Reid, J.; Smith, D. R. Diode laser detection of transient CF3 radicals formed by CO2 laser multiphoton induced dissociation of halocarbons. *Chem. Phys. Lett.* **1987**, *142*, 213–216.

(79) Vakhtin, A. B. The rate constant for the recombination of trifluoromethyl radicals at T = 296 K. *Int. J. Chem. Kinet.* **1996**, *28*, 443–452.

(80) Pagsberg, P.; Jodkowski, J. T.; Ratajczak, E.; Sillesen, A. Experimental and theoretical studies of the reaction between CF_3 and NO_2 at 298 K. *Chem. Phys. Lett.* **1998**, *286*, 138–144.

(81) Dils, B.; Vertommen, J.; Carl, S. A.; Vereecken, L.; Peters, J. The kinetics of the $CF_3 + CF_3$ and $CF_3 + F$ combination reactions at 290 K and at He-pressures of $\approx 1-6$ Torr. *Phys. Chem. Chem. Phys.* **2005**, *7*, 1187–1193.

(82) Skorobogatov, G. A.; Dymov, B. P.; Lebedev, V. N.; Khripun, V. K. Quasi-steady-state pyrolysis of iodotrifluoromethane: kinetics and thermochemistry of trifluoromethyl formation. *Kinet. Catal.* **1987**, *28*, 682.

(83) Skorobogatov, G. A.; Rebrova, A. G.; Khripun, V. K. Rate constant of the recombination of CF_3 radicals in a gas (He, Ar, N_2, or CF_3I). *Kinet. Catal.* **2010**, *51*, 485.

(84) Glaenzer, K.; Maier, M.; Troe, J. Shock-wave study of the high-temperature uv absorption and the recombination of trifluoromethyl radicals. *J. Phys. Chem.* **1980**, *84*, 1681–1686.